Journal of Inorganic and Organometallic Polymers and Materials (2020) 30:2172–2181
https://doi.org/10.1007/s10904-019-01379-7

Uptake of Metal Ions (Co(II) and Ni(II)) by Silica-Salicylaldehyde Derived from Rice Husks

Aliyaa Dhahir Mohsin[1] · **Hayder Hamied Mihsen**[1]

Received: 7 September 2019 / Accepted: 4 November 2019 / Published online: 14 November 2019

Abstract
The source of silica in silica-salicylaldehyde was rice husk ash (RHA). RHA was converted to sodium silicate by reacting with sodium hydroxide solution. The technique of sol–gel was used to synthesize $RHAPrNH_2$ through the reaction of 3-(aminopropyl)triethoxysilane with sodium silicate in a strong acidic medium. Novel nanomaterial (RHA-SALED) was prepared from the reaction of salicylaldehyde with $RHAPrNH_2$ by condensation reaction in toluene solvent. The technique of FTIR showed that the peak at 1622 cm^{-1} belongs to C=N. XRD technique showed the amorphous nature for RHA-SALED with maximum intensity at 22° (2θ). CHNS technique proved that RHA-SALED contain 9.28% of N higher than that of $RHAPrNH_2$. SEM confirmed that the functionalized particles are granular and shaped irregularly with a common diameter of ca. 40.36 nm. BET measurements additionally confirmed that the surface place is 1.0356 $m^2\ g^{-1}$ of RHA-SALED with pore size distribution 10.879 nm. The material RHA-SALED was used for absorption from an aqueous solution of heavy contaminating metal ions Ni(II) and Co(II).

Keywords Rice husk ash · 3-(Aminopropyl)triethoxysilane · Salicylaldehyde · Surface area · Uptake capacity

1 Introduction

Rice is the world's second-largest cereal crop [1]. It is a worldwide food crop presently cultivated in more than 100 countries and approximately 715 million tons of rice paddy is produced each year [2]. Rice husk (RH) is a rich biomass obtained as a by-product during the milling process [3]. Rice husk consists mainly of ash and organic matter consisting of organic cellulose, hemi-cellulose, lignin, and silicon dioxide inorganic [4]. Rice husk is insoluble in water, it has excellent chemical stability and structural strength owing to its elevated silica content [5]. Rice husk ash (RHA) is a silica-rich agriculture waste material, typically 90–95 wt% amorphous SiO_2. It is possible to produce amorphous RHA at temperatures up to 800 °C [6]. The principal element of rice husk ash is silicon (87.7% as SiO_2), followed by potassium (5.4% as K_2O) and phosphorous (3.7% as P_2O_5) [7]. Rice husk ash is used as a supplementary material for the manufacturing of cement and concrete cubes. It is also used as soil stabilization additives as an adsorbent for contaminant removal from contaminated water and wastewater [8]. Silica is the richest oxide in the earth crust [9]. With its excellent stability, high surface area, chemical purity, strong adsorption and good dispersing capability, Silica has also gained great attention with desirable properties. Many researchers investigated the potential of rice husk as an outstanding source of high-grade amorphous silica that can be obtained by comparatively easy techniques [10–13]. Heavy metals are common land and water pollutants that can be unintentionally discharged from a variety of industries such as electroplating, battery storage and mining. Because of the significant adverse effects on human health and the natural environment [14]. The term heavy metals is commonly defined for those metals that have specific weights greater than 5 g cm^{-3} [15]. Thus, studies have been carried out in latest years to discover more efficient and cheaper ways to remove heavy metal ions from aqueous effluent. A wide variety of techniques have been developed to remove these metal ions from wastewater such as exchange of ions, inverse osmosis, adsorption, precipitation, co-precipitation, filtration and coagulation. Due to simplicity and low cost, the adsorption method is very common and

✉ Hayder Hamied Mihsen
hayderalhmedawy@gmail.com

[1] Department of Chemistry, College of Science, University of Kerbala, Karbala, Iraq

effective, several materials of adsorption can capture metal ions from aqueous solutions [16–20]. Numerous research has therefore concentrated on porous adsorbents that have demonstrated important improvements in the effective removal of heavy metals. Mesoporous materials with a large surface area and uniform distribution of pores were extensively studied in the fields of adsorption, catalysis, sensors, semiconductors and separation [21]. Because they are non-toxic and biocompatible, silica-based materials are considered to be the finest adsorbents available [22]. Hybrid silica-based solid supports incorporated with chelating groups have many applications in fields such as extraction, regeneration and separation of metal ions from aqueous solutions as well as stationary chromatographic phases and heterogeneous catalysis [23–26]. The bi-functional polysiloxanes immobilized ligand systems provide a wide range and high ability for various kinds of metal ions from aquatic media [27]. In this paper, the inorganic–organic hybrid nanomaterial (RHA-SALED) is synthesized from rice husk ash and used it for extracted metal ions (Co(II) and Ni(II)) from its aqueous solutions.

2 Experimental Part

2.1 Materials

The rice husks were collected from a local factory for rice production in Najaf Governorate-Abbasiya city. Sodium hydroxide (BHD, England 99%), 3-aminopropyltriethoxysilane (Sigma, 99%), Nitric acid (CDH, India 70%), Salicylaldehyde (CDH, India 99%), Toluene (Merk, KGaA, Germany 99%), Acetone (Romal 99.7%), Cobalt chloride hexahydrate (BDH, England 97%), Nickel chloride hexahydrate (BDH, England 96%) are all chemicals that have been used as received without further purification.

2.2 Samples Characterization

The FT-IR spectra were registered on a Shimadzu 8400 spectrophotometer with specimens in the KBr in the range of 4000–400 cm^{-1}. The patterns of X-ray diffraction (XRD) were examined using Shimadzu X-ray diffractometer. CHNS elemental analysis was performed on an (Eager 300 for EA1112). SEM analysis was performed on a FESEM MIRA III (TESCAN). The samples were suspended 10 min before analyzing in ethanolic solution. BEL BELSORP MINI II instrument was used to measure the nitrogen adsorption/desorption analysis. Thermogravimetric analysis (TGA/DTA) was carried out using the instrument SDT Q600 V20.9 Build 20.

2.3 Synthesis of Amorphous Silica from Rice Husk

The amorphous silica (rice husk ash (RHA)) was synthesized from rice husk according to the procedure previously described in [26, 28–30].

2.4 Synthesis of Functionalized Silica with 3-(Aminopropyl)triethoxysilane (APTES)

Rice husk ash was functionalized with 3-(aminopropyl)triethoxysilane (APTES) to prepare $RHAPrNH_2$ according to the procedure described by Adam.et al. [31].

2.5 Synthesis of Silica-Salicylaldehyde Nanomaterial, RHA-SALED

1 g of $RHAPrNH_2$ was added to an excess of salicylaldehyde of about (3 mL) and the mixture was refluxed with 30 mL of toluene for 48 h. The yellow solid product was filtered and washed with an amount of DMSO, ethanol and acetone. The solid product was dried at 110 °C for 24 h. Finally, 1.4 g of powder was collected and labeled as RHA-SALED. The overall preparation steps have been shown in Scheme 1.

2.6 Experiments of Metal Uptake

An amount of 100 mg of RHA-SALED was shaken with (50 mL, 0.05 M) of aqueous metal(II) ion solution (Co(II) and Ni(II)) in a plastic container. Uptake concentration of metal ion were measured by withdraw 5 mL of metal solution containing solid ligand RHA-SALED using a filtered syringe to remove solid particles and diluted for the linear range of the calibration curve. Uptake concentration (Cu) of metal ion was calculated by subtract residual concentration(Cr) (after addition RHA-SALED) from initial concentration (Ci), according to this equation: $Cu = Ci - Cr$.

Optimization conditions such as shaking time, pH effect, metal concentration and solid ligand mass (RHA-SALED) were examined.

3 Results and Discussion

3.1 FTIR Spectroscopy Analysis

The FT-IR spectra of RHA and $RHAPrNH_2$ were discussed previously [21]. The FT-IR spectra of RHA, $RHAPrNH_2$ and RHA-SALED are shown in Fig. 1. A broad absorption band around 3400 cm^{-1} was assigned to hydroxyl group in aromatic moiety and silanol groups(Si–OH) that adsorbed water molecules on the silica surface [32]. The band at

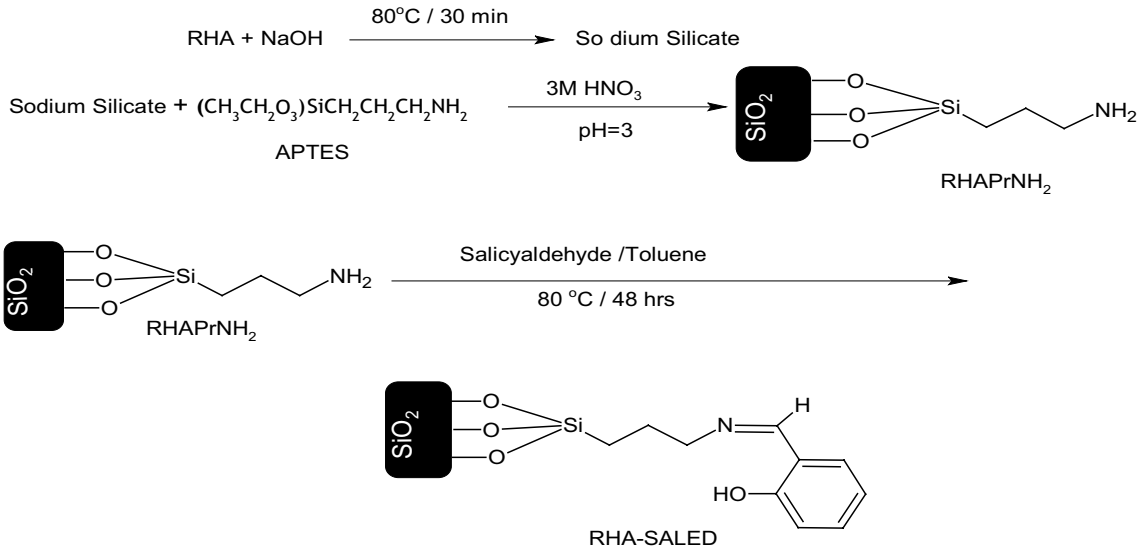

Scheme 1 The synthesis steps of RHA-SALED

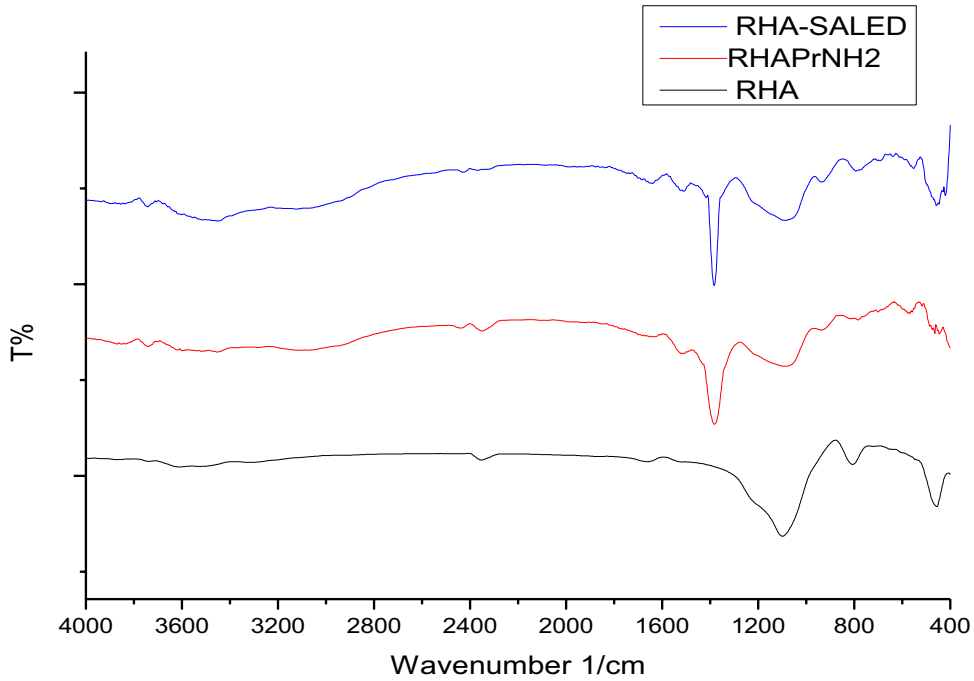

Fig. 1 FT-IR spectra of RHA, $RHAPrNH_2$ and RHA-SALED

3022 cm^{-1} was assigned to the C–H aromatic stretching vibration [26]. FT-IR spectrum also exhibits bands at 475, 900 and 1100 cm^{-1}, characteristic of symmetric and anti-symmetric stretching of Si–O–Si bonds [33]. The stretching vibration assigned to azomethine group C=N appeared at 1622 cm^{-1} [25].

3.2 XRD Diffraction Pattern

XRD analysis revealed wide peaks diffused with maximum intensity at $2\theta = 22°$, and sharp peaks were absent in Fig. 2 indicating high purity for prepared material, indicating the amorphous structure of the RHA-SALED analyzed. Amorphous is also characterized by peaks in the 2θ range of 15–30° [34, 35]. The mean crystal size of RHA-SALED was calculated from XRD data, which depended onto Deby–Scherrer formula and found to equal to 1.266 nm [36].

3.3 Elemental Analysis CHNS

Elemental analysis of RHA, RHA-$PrNH_2$ and RHA-SALED are shown in Table 1. RHA-SALED contains 9.28% of N

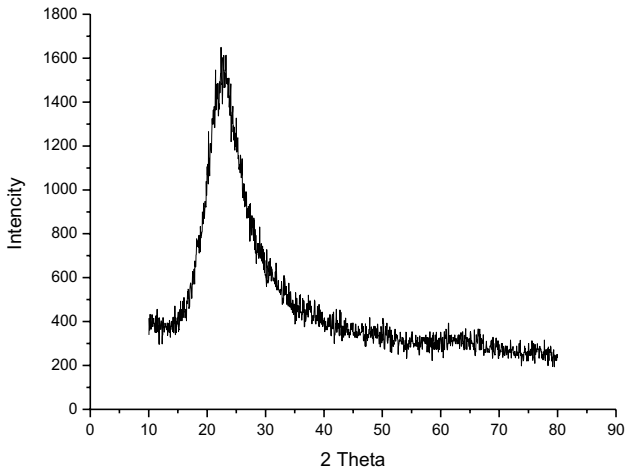

Fig. 2 The X-ray diffraction pattern shows amorphous nature of RHA-SALED

Table 1 Chemical analysis of RHA, $RHAPrNH_2$ and RHA-SALED using of elemental analysis

Sample	C (%)	H (%)	N (%)	S (%)
RHA [37]	1.6	0.84	–	–
$RHAPrNH_2$ [31]	9.67	2.31	6.08	–
RHA-SALED	11.82	3.37	9.28	–

higher than that of $RHAPrNH_2$, and the percentage of C and H for RHA-SALED are significantly higher than that of both $RHAPrNH_2$ and RHA, as was expected. These results clearly indicate the successful immobilization of RHA-SALED onto $RHAPrNH_2$ [26].

3.4 SEM–EDX Analysis

The SEM images of RHA-SALED are shown in Fig. 3. The microphotographs obtained indicate that the particles of RHA-SALED analyzed were irregularly shaped. It is also confirmed that all samples have wide granulometric distribution [34] with an average diameter of ca. 40.36 nm.

Figure 4 illustrates the spectrum for EDX of RHA-SALED showing nitrogen and other elements in the solid ligand, which indicates that the RHA-SALED was incorporated on the $RHAPrNH_2$.

3.5 Nitrogen Adsorption Desorption Analysis

Figure 5 shows the nitrogen adsorption isotherm obtained for RHA-SALED. The pore size distribution is shown inset. The hysteresis loop was observed in the range of $0.55 < P/Po < 0.97$, associated with capillary condensation according to IUPAC classification. The isotherm shown was of the type IV and exhibited an H3 hysteresis loop. The BET analysis exhibited that the specific surface area of RHA-SALED was 1.0356 $m^2\ g^{-1}$, while the specific surface area of $RHAPrNH_2$ was reported to be 1.32 $m^2\ g^{-1}$. However, the decrease in the surface area of RHA-SALED, could be due to the reduction of the surface sites due to the immobilization of salicylaldehyde on silica surface, causing the surface to be over crowded with the ligand network on the surface and thus blocking the pores [38]. The average pore volume and average pore diameter of RHA-SALED was found to be 0.0028 $cm^3\ g^{-1}$ and 10.87 nm, respectively (Table 2).

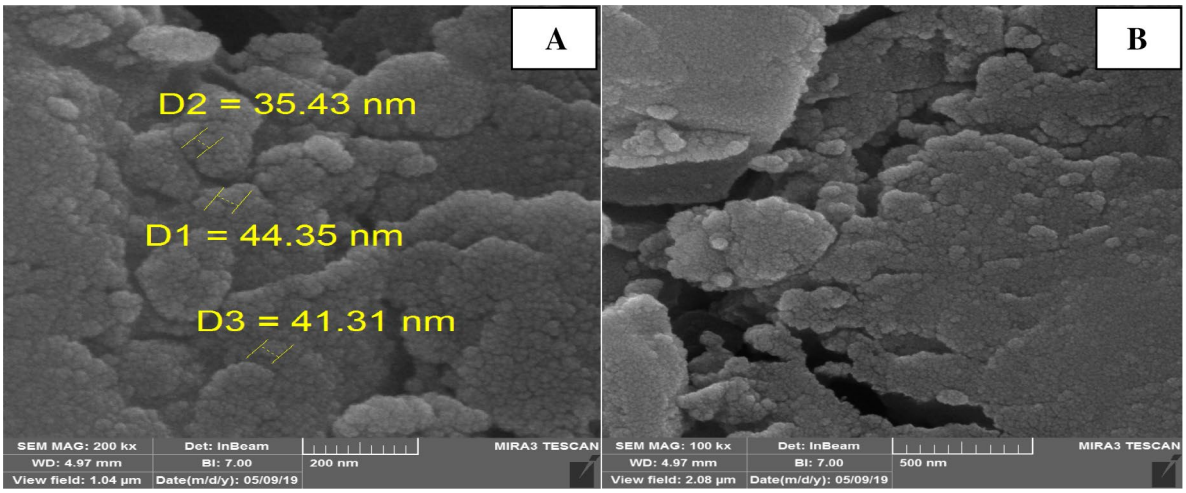

Fig. 3 The SEM micrographs of RHA-SALED (**a** 200 nm and **b** 500 nm)

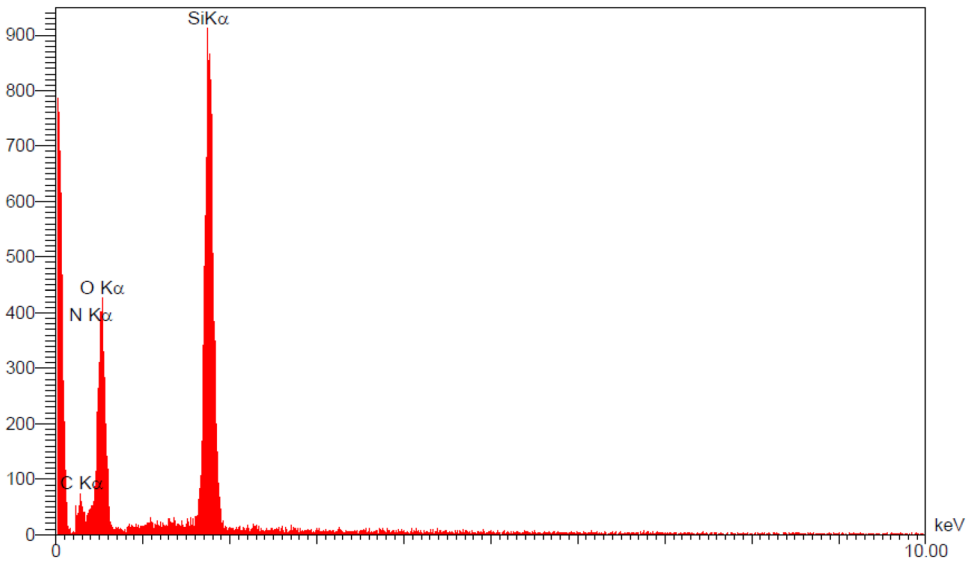

Fig. 4 EDX chart for RHA-SALED

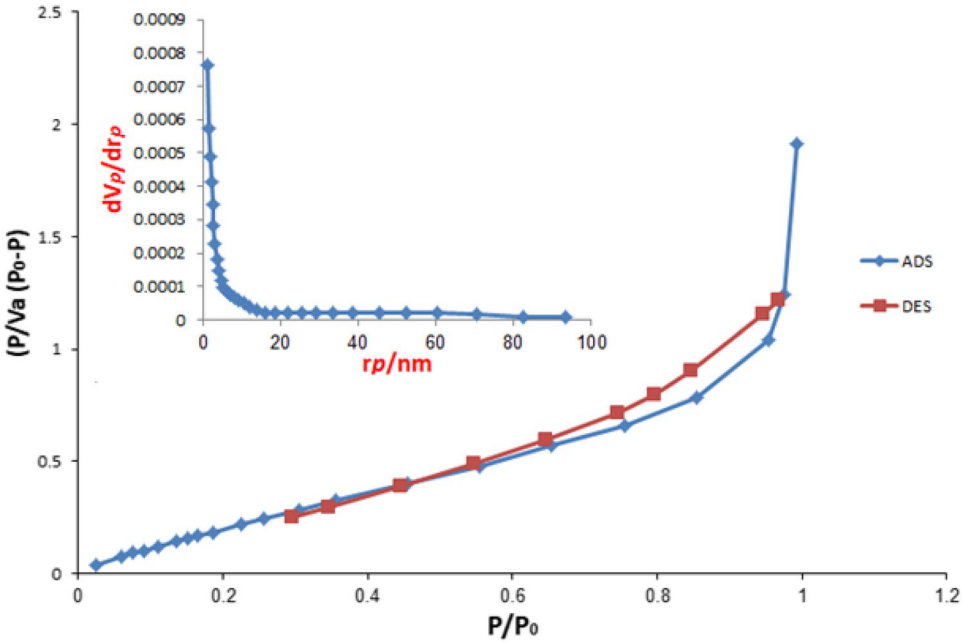

Fig. 5 The nitrogen adsorption–desorption isotherms and pore size distribution of RHA-SALED

Table 2 Result of BET analysis for RHA, $RHAPrNH_2$ and RHA-SALED

Sample	Specific surface area/(m^2 g^{-1})	Average pore volume/(cm^3 g^{-1})	Average pore diameter/nm
RHA [39]	347	0.872	10.40
$RHAPrNH_2$ [31]	1.32	0.0053	3.52
RHA-SALED	1.0356	0.0028	10.87

3.6 Thermal Analysis

The thermogravimetric analysis TGA/DTA was performed in the range of 25–600 °C. Figure 6 shows TGA/DTA of the RHA-SALED which illustrates two characteristic decomposition stages. The initial step showed mass loss (ca. 15.62%) at 25–175 °C with a maximum at 117 °C. This loss is attributed to the absorbed water onto the surface of silica. The second mass loss (ca. 46.87%) occurred between 175 and 300 °C, with a maximum at 240 °C assigned to the decomposition of azomethine group and phenol moiety. The third mass loss (ca. 37.50%) occurred between 300 and 600 °C and is attributed to the remaining decomposition of

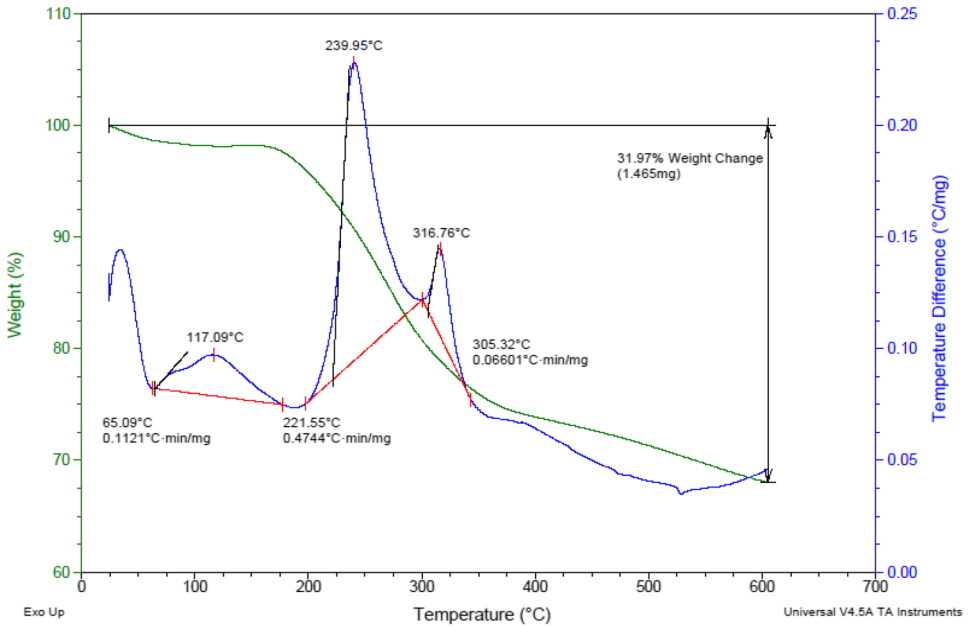

Fig. 6 The thermogravimetric analysis for RHA-SALED

the remaining organic part and also to the decomposition of silanol groups.

3.7 Metal Uptake Experiments

3.7.1 Effect of Shaking Time on the Metal Uptake

The capability of metal ion uptake for ions (Ni(II) and Co(II)) was determined by the shaking ligand (RHA-SALED) in aqueous divalent metal ion solution for 24 h at different time intervals. The results are given in Fig. 7. It is shown that the uptake of metal ions increases in a nonlinear fashion as a function of exposure time. The rise in the uptake of metal ions over time is due to diffusion factors. The metal ion uptake process increased rapidly in the initial hours, then after 4 h it became very slow, this may be due to solid metal ion ligand saturation. It was observed that there was no change in the uptake of Co(II) and Ni(II) ions when the shaking time was increased over 4 h. Hence the uptake process equilibrium time over RHA-SALED is 4 h.

3.7.2 Effect of pH

The impact of the pH parameter on the metal ion uptake process by RHA-SALED was studied at four different pH values. Results from these parameters are given in Figs. 8

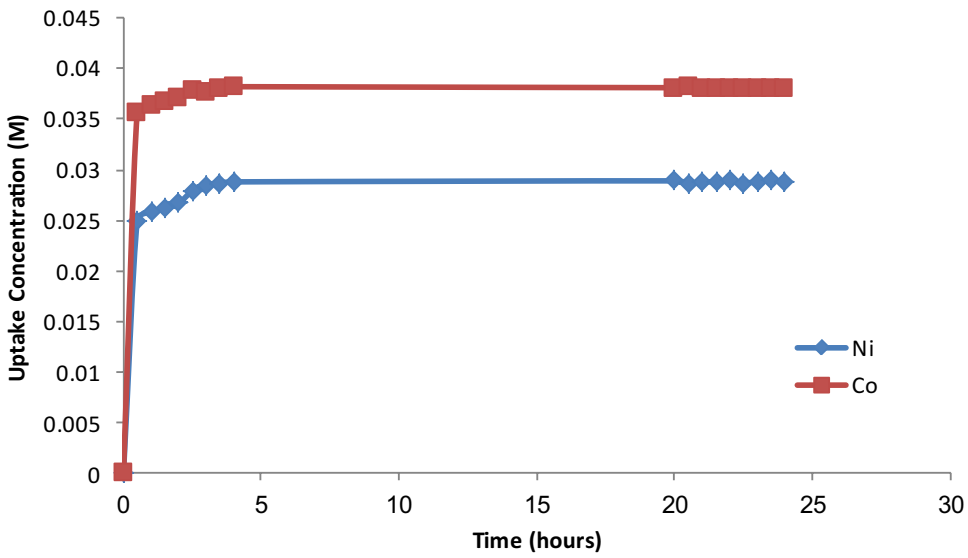

Fig. 7 The uptake of Ni(II) and Co(II) ions by RHA-SALED versus time

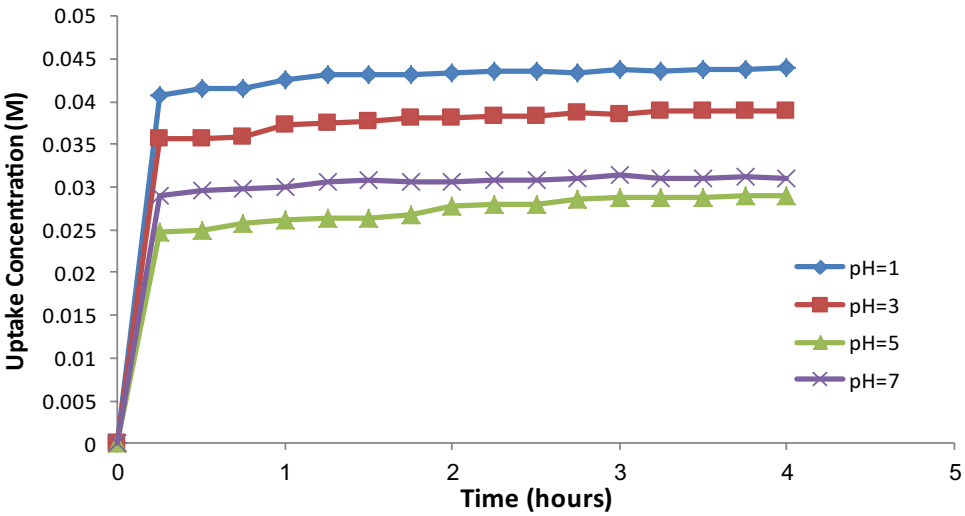

Fig. 8 The uptake of Ni(II) ions by RHA-SALED with various pH of Ni(II) ions solution versus time of reaction

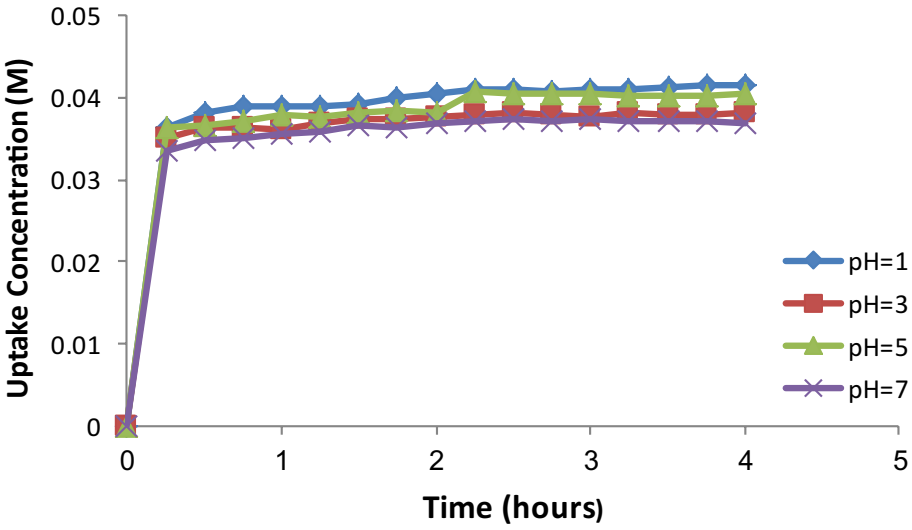

Fig. 9 The uptake of Co(II) ions by RHA-SALED with various pH of Co(II) ions solution versus time of reaction

and 9. The metal capacity increased as the pH decreased and reached its maximum at pH = 1 for Co(II) and Ni(II) ions. High pH values were not studied due to hydroxide formation [24].

3.7.3 Effect of the Initial Concentration of Metal Ion Solution

The impact of the original concentration of Ni(II) and Co(II) ions was explored by taking 0.1 g of RHA-SALED and shaking solutions for 4 h using different concentrations Ni(II) and Co(II) ions (0.02, 0.05 and 0.08 M). The results, exhibited in Figs. 10 and 11, indicate that the uptake capability improves as the original concentration of metal ion solution increases. Maximum uptake occurs at concentration of 0.08 M. It is shown that the nickel uptake concentration increased from 0.0159 M at initially to 0.0638 M at 4 h, while the cobalt uptake concentration increased from 0.0126 M initially to 0.0659 M at 4 h. There was no change in the uptake concentration after 4 h due to the saturated RHA-SALED of Ni(II) and Co(II) ion concentrations. The ability for uptake of heavy metal increased with an increase in the concentration of metal ions. This may be due to high driving power of the increased concentration of metal ions.

3.7.4 Effect of the Mass of the Functionalized Silica

The impact of the functionalized silica mass using three different ligand masses (100, 150, and 200 mg) was investigated. Figures 12 and 13 illustrate the uptake capacity of RHA-SALED for Ni(II) and Co(II) ions, respectively. The results obtained showed that the maximum uptake capacity increased for both Ni(II) and Co(II) ions as the ligand mass decreased. The large mass of RHA-SALED, however, lowers the uptake capacity. This can be due to block of donor sites of solid ligand by the ligand itself.

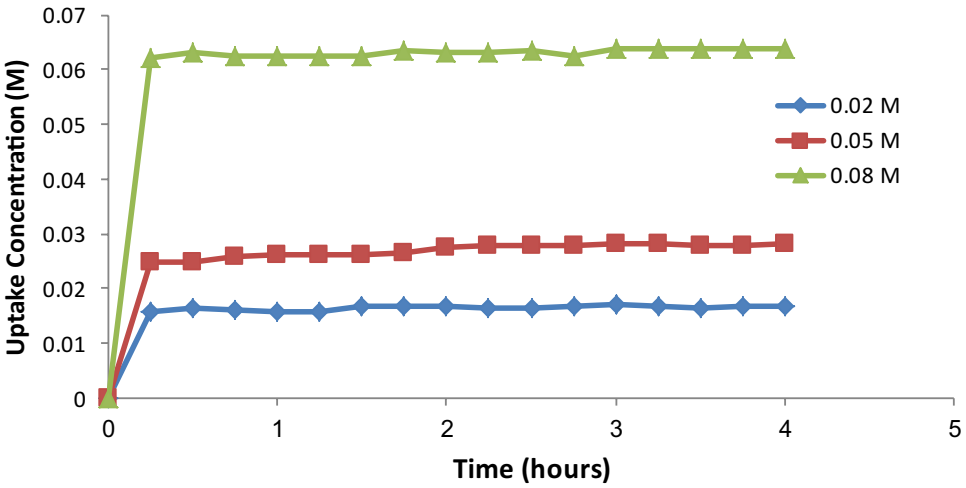

Fig. 10 The uptake of Ni(II) ions by RHA-SALED with various initial concentration of the Ni(II) ions versus time of reaction

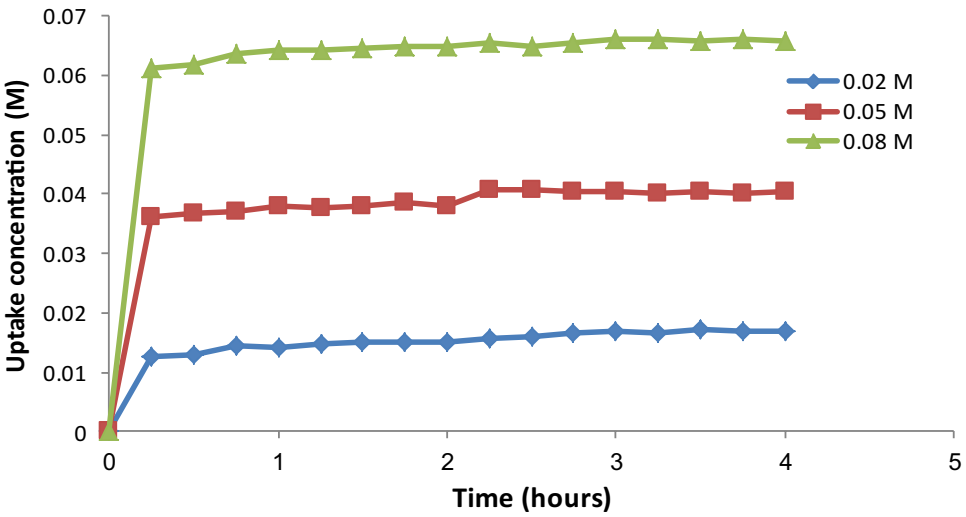

Fig. 11 The uptake of Ni(II) ions by RHA-SALED with various initial concentration of Ni(II) ions versus the time of reaction

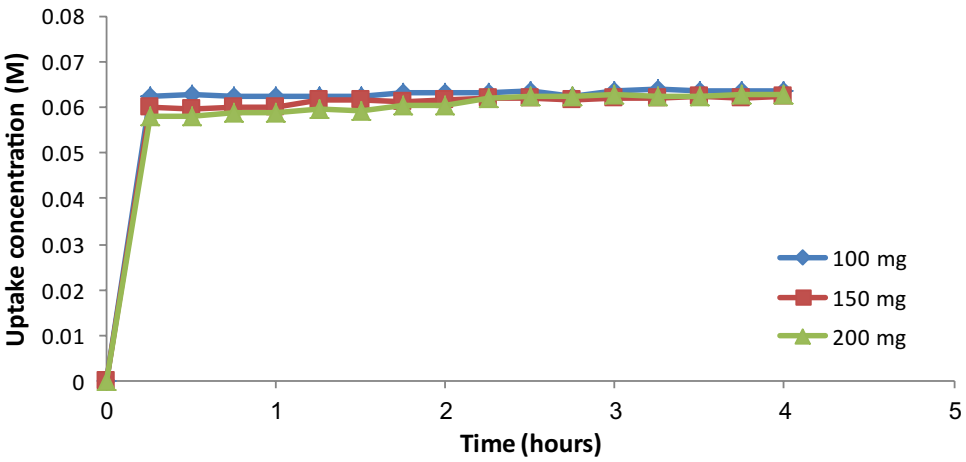

Fig. 12 The uptake of Ni(II) ions by RHA-SALED with various masses of the ligand versus the time of reaction

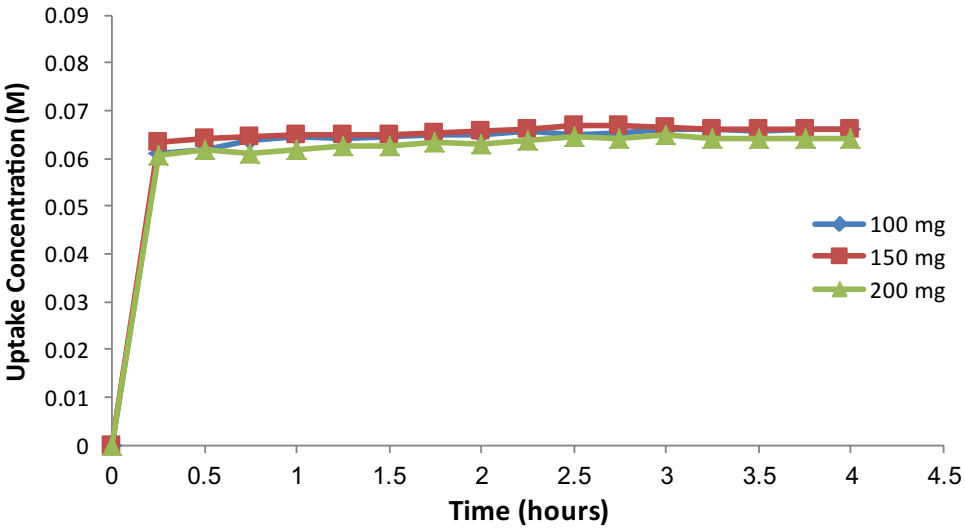

Fig. 13 The uptake of Co(II) ions by RHA-SALED with various masses of the ligand versus the time of reaction

4 Conclusions

RHA-SALED was synthesized using condensation reaction between silica source ($RHAPrNH_2$) and salicylaldehyde. Many physical techniques such as FT-IR, BET, XRD, CHNS, FESEM and TGA/DTA analyses have been used for characterization of prepared material. The spectra of FT-IR were showed the presence of C=N on RHA-SALED. The BET analysis was indicated the reduction of the surface area for RHA-SALED due to the immobilization of organic molecule (salicylaldehyde) on the silica surface. The XRD diffraction pattern shows that the RHA-SALED has amorphous nature. Elemental analysis proved that RHA-SALED contains carbon and nitrogen higher than that of RHAPrNH2. The TGA/DTA thermogravimetry analysis shows that the RHA-SALED could be stable and it may decompose in between 170 and 300 ℃. The solid ligand system RHA-SALED exhibits high efficiency to remove and extraction Ni(II) and Co(II) ions from their aqueous solution.

Acknowledgements We would like to thank Department of Chemistry, College of Science, Kerbala University, for financial support.

References

1. S. Azat, A.V. Korobeinyk, K. Moustakas, V.J. Inglezakis, J. Clean. Prod. **217**, 352 (2019)
2. F. Requena, R. Jiménez-Quero, A. Vargas, M. Moriana, R. Chiralt, A. Vilaplana, A.C.S. Sustain, Chem. Eng. **7**, 6275 (2019)
3. M. Ullah, Z. Man, Z. Khan, A.S. Muhammad, N. Mahmood, H. Ghanem, O.B. Raheel, J. Clean. Prod. **220**, 620 (2019)
4. M.F. De Souza, W.L.E. Magalhães, M.C. Persegil, Mater. Res. **5**, 467 (2002)
5. D. Sivakumar, Glob. J. Environ. Sci. Manag. **1**, 27 (2015)
6. P. Sturm, G.J.G. Gluth, H.J.H. Brouwers, H.-C. Kühne, Constr. Build. Mater. **124**, 961 (2016)
7. H.X. Nguyen, N.T.T. Dao, H.T.T. Nguyen, A.Q.T. Le, in *IOP Conference Series: Earth and Environmental Science* (2019), p. 12007
8. M. Beidaghy, D.H. Zeng, T. Hartmann, I. Enke, D. Schliermann, T. Lenz, V. Bidabadi, Appl. Sci. **9**, 1083 (2019)
9. J.T. Librea, F.D. Dacanay, Z.Z. Martin, L.L. Diaz, in *IOP Conference Series: Earth and Environmental Science* (2019), p. 12007
10. S. Sembiring, R. Situmeang, Z. Sembiring, Cerâmica **65**, 194 (2019)
11. C. Real, M.D. Alcala, J.M. Criado, J. Am. Ceram. Soc. **79**, 2012 (1996)
12. R.A. Bakar, R. Yahya, S.N. Gan, Procedia Chem. **19**, 189 (2016)
13. J.A. Santana Costa, C.M. Paranhos, J. Clean. Prod. **192**, 688 (2018)
14. X. Xu, Y. Zheng, B. Gao, X. Cao, Chem. Eng. J. **368**, 564 (2019)
15. J. Acharya, U. Kumar, P.M. Rafi, Int. J. Curr. Eng. Technol. **3**, 525 (2018)
16. M. Najafi, Y. Yousefi, A.A. Rafati, Sep. Purif. Technol. **85**, 193 (2012)
17. Y. Liu, H. Feng, S. Zhang, N. Du, X. Liu, Front. Environ. Sci. Eng. **8**, 329 (2014)
18. S.K. Gunatilake, Methods **1**, 12 (2015)
19. S. Naushad, M. Ahamad, T. Al-Maswari, B.M. Alqadami, A.A. Alshehri, Chem. Eng. J. **330**, 1351 (2017)
20. Z. An, F.Q. Wu, R.Y. Li, M. Hu, T.P. Gao, J.F. Yuan, React. Funct. Polym. **118**, 42 (2017)
21. G. Li, Z. Zhao, J. Liu, G. Jiang, J. Hazard. Mater. **192**, 277 (2011)
22. S. Ahmad, N. Sereshti, H. Mousazadeh, M. Nodeh, H.R. Kamboh, M.A. Mohamad, Mater. Chem. Phys. **226**, 73 (2019)
23. J. El-Ashgar, N.M. El-Nahhal, I.M. Chehimi, M.M. Babonneau, F. Livage, Int. J. Environ. Anal. Chem. **89**, 1057 (2009)
24. I.M. El-Nahhal, F.R. Zaggout, N.M. El-Ashgar, Anal. Lett. **33**, 2031 (2000)
25. I.M. El-Nahhal, N.M. El-Ashgar, J. Organomet. Chem. **692**, 2861 (2007)
26. T.J. Al-Hasani, H.H. Mihsen, K.M. Hello, F. Adam, Arab. J. Chem. **10**, S1492 (2017)
27. M.M. El-Ashgar, N.M. El-Nahhal, I.M. Ahmed, M.A. Shaweesh, A.A.A. Chehimi, J. Iran. Chem. Soc. **15**, 2325 (2018)
28. K.M. Hello, H.H. Mihsen, M.J. Mosa, Iran. J. Catal. **4**, 195 (2014)
29. K.M. Hello, H.H. Mihsen, M.J. Mosa, M.S. Magtoof, J. Taiwan Inst. Chem. Eng. **46**, 74 (2015)
30. H.H. Mihsen, H.S. Sobh, Asian J. Chem. **30**, 937 (2018)

31. F. Adam, K.M. Hello, H. Osman, Chin. J. Chem. **28**, 2383 (2010)
32. T. Chanadee, S. Chaiyarat, J. Mater. Environ. Sci. **7**, 2369 (2016)
33. J.M. Carmona, V.B. Oliveira, R.M. Silva, W.T.L. Mattoso, L.H.C. Marconcini, Ind. Crops Prod. **43**, 291 (2013)
34. R. Fernandes, I.J. Calheiro, D. Kieling, A.G. Moraes, C.A. Rocha, T.L. Brehm, F.A. Modolo, Fuel **165**, 351 (2016)
35. S.R. Kamath, A. Proctor, Cereal Chem. **75**, 484 (1998)
36. M.J. Barnabas, S. Parambadath, S. Nagappan, C.S. Ha, Heliyon **5**, e01521 (2019)
37. F. Adam, H. Osman, K.M. Hello, J. Colloid Interface Sci. **331**, 143 (2009)
38. F. Adam, K.M. Hello, S.J. Chai, Chem. Eng. Res. Des. **90**, 633 (2012)
39. A.E. Ahmed, F. Adam, Microporous Mesoporous Mater. **103**, 284 (2007)